N-Heterocyclic Olefins   Hot Paper

N-Heterocyclic Olefins on a Silicon Surface

Mowpriya Das+, Conor Hogan+, Robert Zielinski, Milan Kubicki, Maximilian Koy,
Canan Kosbab, Simone Brozzesi, Ankita Das, Mike Thomas Nehring, Viktoria Balfanz,
Juls Brühne, Mario Dähne, Martin Franz,* Norbert Esser,* and Frank Glorius*

Abstract: The adsorption of N-heterocyclic olefins (NHOs) on silicon is investigated in a combined scanning tunneling microscopy, X-ray photoelectron spectroscopy, and density functional theory study. We find that both of the studied NHOs bind covalently, with ylidic character, to the silicon adatoms of the substrate and exhibit good thermal stability. The adsorption geometry strongly depends on the N-substituents: for large N-substituents, an upright adsorption geometry is favored, while a flat-lying geometry is found for the NHO with smaller wingtips. These different geometries strongly influence the quality and properties of the obtained monolayers. The upright geometry leads to the formation of ordered monolayers, whereas the flat-lying NHOs yield a mostly disordered, but denser, monolayer. The obtained monolayers both show large work function reductions, as the higher density of the flat-lying monolayer is found to compensate for the smaller vertical dipole moments. Our findings offer new prospects in the design of tailor-made ligand structures in organic electronics and optoelectronics, catalysis, and material science.

[*]   Dr. M. Das,+ Dr. M. Koy, A. Das, Prof. Dr. F. Glorius
      Westfälische Wilhelms-Universität Münster, Organisch-Chemisches
      Institut, Corrensstrasse 40, 48149 Münster (Germany)
      E-mail: glorius@uni-muenster.de

      Dr. C. Hogan+
      Istituto di Struttura della Materia-CNR (ISM-CNR), Via del Fosso
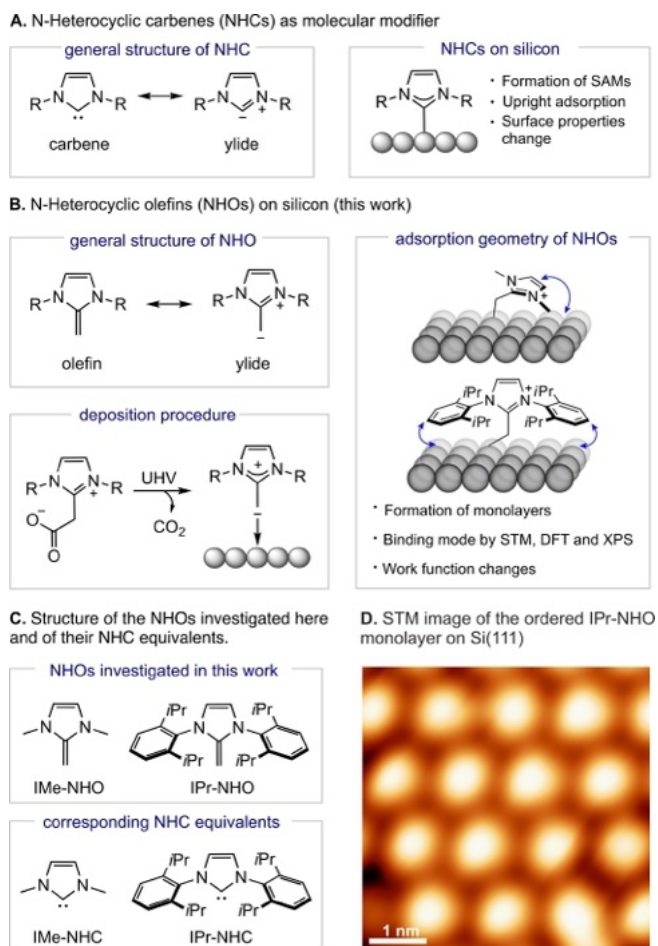   del Cavaliere 100, 00133 Rome (Italy)

      Dr. C. Hogan,+ S. Brozzesi
      Dipartimento di Fisica, Università di Roma 'Tor Vergata', Via della
      Ricerca Scientifica 1, 00133 Rome (Italy)

      R. Zielinski, M. Kubicki, C. Kosbab, M. T. Nehring, V. Balfanz,
      J. Brühne, Prof. Dr. M. Dähne, Dr. M. Franz, Prof. Dr. N. Esser
      Technische Universität Berlin, Institut für Festkörperphysik,
      Hardenbergstrasse 36, D-10623 Berlin (Germany)
      E-mail: martin.franz@physik.tu-berlin.de

      Prof. Dr. N. Esser
      Leibniz-Institut für Analytische Wissenschaften – ISAS e.V.,
      Schwarzschildstrasse 8, 12489 Berlin (Germany)
      E-mail: norbert.esser@isas.de

[+]   These authors contributed equally.

Introduction

Owing to the ever-growing number of applications for semiconductor materials, it becomes increasingly imperative to modify surfaces that enable the creation of highly tailored and advanced materials. Silicon, upon which the modern semiconductor industry is largely based, is one of the most sought-after materials in this regard. Therefore, new approaches to functionalize and tune silicon surfaces are particularly desired and molecular modifiers have emerged as a novel toolkit in the field.[1,2]

N-Heterocyclic olefins (NHOs) are a class of compounds containing a terminal alkylidene unit formally attached to an N-heterocyclic carbene (NHC) (see Figure 1A,B).[3] NHOs feature an exceptionally electron rich and strongly polarizable double bond best represented by two resonance structures: a neutral olefin and a zwitterionic ylide. As a result, the terminal carbon atom generally shows high nucleophilicity.[4] After their successful isolation in 1993, NHOs were used for the stabilization of various transition metals and main group species including first applications in catalysis.[3,5–10] In addition, NHOs are structurally similar to the "deoxy-Breslow" intermediates formed during certain NHC-organocatalyzed reactions.[11–15] First studies show their strong σ-donor ability with the absence of π-backbonding properties.[16] As a result NHOs tend to show weaker coordination to metal centers compared to the corresponding NHCs.[17,18] Single crystal X-ray crystallography of NHO transition metal complexes generally prove end-on coordination via the ylide form.[8,16]

Interestingly, surface modification by NHOs has — to the best of our knowledge — not been reported yet. This is in stark contrast to their close relatives, the NHCs, which have proven to be excellent ligands for surface modification with applications in the fields of materials science and catalysis.[21–52] Recently, also the use of N-heterocyclic carbenes as molecular modifiers for silicon surfaces has been reported (see Figure 1A). NHCs bind covalently to Si(111) via single Si–C bonds which lead to thermally stable monolayers and a significant reduction of the work function compared to the unfunctionalized surface.[19,20,53] A strong dependence of the order of the monolayer on the nature of the N-substituents was found with bulky aromatic substituents leading to highly ordered monolayers.

For NHOs, multiple binding modes either via end-on coordination best represented by the ylidic form or side-on coordination via the neutral olefinic resonance structure could be envisioned and could potentially lead to novel

Figure 1. (A) NHCs as molecular modifiers for silicon surfaces. The formation of ordered monolayers on silicon has previously been demonstrated.[19,20] (B) Surface modification using NHOs remains unexplored. This study examines the formation of monolayers and the binding modes of different NHOs on silicon. The blue arrows indicate the interaction between the surface and the rings. (C) Structure of the NHOs studied herein, and their NHC equivalents. (D) STM image of the ordered IPr-NHO monolayer.

For the model NHOs studied in this work (Figure 1C), different binding modes are observed depending on the presence or absence of bulky N-substituents (wingtips), leading to different local geometries, surface assembly, and electronic properties. For IPr-NHO, a well ordered monolayer is obtained as shown in Figure 1D being an important prerequisite for applications, e.g. in organic field effect transistors.[63] In the future, a tailor-made surface functionalization is conceivable by targeted modification of the employed NHOs, e.g. their N-substituents or in the backbone. Both NHO monolayers are characterized by large work function reductions demonstrating dramatic changes in the electronic structure. As at least one low work function material is necessary in a variety of devices, e.g. organic light emitting diodes or organic photovoltaic devices, this opens up interesting possibilities for applications of NHO functionalized surfaces.[2,64–66]

Results and Discussion

In order to identify the most stable adsorption geometries for the two NHOs we performed density functional theory (DFT) simulations. In the following, we denote the C atom in the exocyclic group as C_{exo} and the terminal C atom within the heterocyclic ring as C_{endo} (the latter corresponds to the divalent C in NHCs). As shown in Figure 2, we find both NHOs decisively bind to the Si adatom via the C_{exo} atom. The adsorption energies of single molecules (computed using a $4\sqrt{3} \times 4\sqrt{3}$ cell) are -1.82 eV for IMe-NHO and -1.98 eV for IPr-NHO, indicating chemisorption, and

properties and assembly behavior as a result of the different geometrical and electronic characteristics of NHOs compared to NHCs.
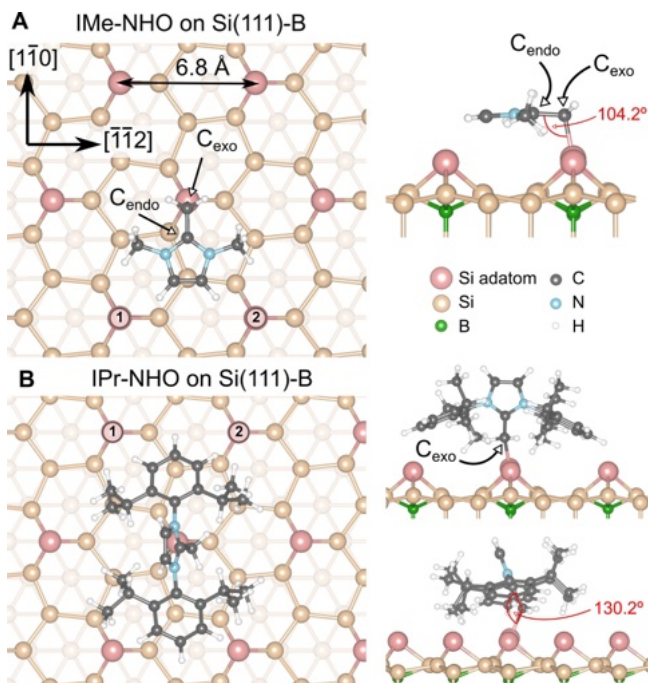
Herein, we deposited two NHO molecules with structurally different N-substituents. We choose CO_2 adducts of NHOs as precursors due to higher stability and easier handling in comparison to the free NHOs. Thermally induced decarboxylation then leads to free NHOs for vapor deposition on the anticipated surface (see Figure 1B and section 1.3 of the Supporting Information).[26,27]

The Si(111)$\sqrt{3} \times \sqrt{3}$R30°-B surface (Si(111)-B) was chosen as a substrate as it has been demonstrated to be particularly suitable for the self-assembly of organic films.[19,20,54–60] On this surface, the otherwise highly reactive dangling bond sites are deactivated due to the subsurface incorporation of B atoms.[61,62] The structure model and scanning tunneling microscopy (STM) results of the clean Si(111)-B surface are presented in Figure S1.

Figure 2. Optimized geometries of (A) IMe-NHO and (B) IPr-NHO on the Si(111)-B surface, as predicted by DFT. Top views and side views along the [$\bar{1}\bar{1}2$] (and [$1\bar{1}0$]) direction are shown.

are thus comparable with the values found for the corresponding NHCs (-1.93 eV and -2.48 eV). Alternative geometries (e.g. pure physisorption) were not found to be stable.

In contrast to our findings for NHCs on Si(111)-B,[19] which tend to adsorb upright, the smaller IMe-NHO molecule assumes a flat-lying geometry. This allows C_{exo} to approach an sp^3-like geometry ($104.2°\sim109.5°$) and maximize the energetic contribution from vdW coupling with the substrate (-0.61 eV). The Si–C bond is also slightly longer for the NHO form (2.00 Å vs. 1.92 Å for IMe-NHC). The large side groups in IPr-NHO instead prevent its inner ring from adopting a flat-on alignment, while providing a large vdW contribution (-1.31 eV) to the adsorption energy. To mitigate the strain on the exocyclic group, the Si–C_{exo} bond is tilted by $24.9°$ away from the surface normal, and the bond angle $\angle$Si–C_{exo}–C_{endo} lowers to $130.2°$. The IPr-NHO central ring is therefore not perfectly upright like in the NHC case, but is ultimately tilted by $26.2°$ from the surface normal. Despite the clear difference in binding modes, however, all bond lengths (including Si–C_{exo}) differ by (at most) 0.01 Å between the two molecules, suggesting the final electronic and chemical character of the bond is independent of the NHO.

The azimuthal orientation of the molecules on the substrate is governed by steric interactions with neighboring Si adatoms. Our DFT calculations of the energy dependence on rotation angle (Figure S2) reveal that IMe-NHO tends to align such that the backbone falls between two Si adatoms (marked 1 and 2 in Figure 2), yielding six equivalent orientations. The rotational barrier is very low (66 meV) suggesting free movement at room temperature. A similar situation occurs for IPr-NHO, as the side-groups tend to align between Si adatom pairs. In this case, however, a true sixfold degeneracy is not present due to a small energetic dependence on the direction of the Si–C_{exo} bond (threefold substrate symmetry). The barrier for rotation is markedly higher at 220–250 meV.

We now turn to the discussion of the experimental measurements. Figures 3A and C show overview STM images for low coverages of IPr-NHO and IMe-NHO, respectively. As all experimental results presented in this work, the images were acquired at room temperature. The molecules appear as bright spots distributed randomly across the surface. In between the molecules the substrate surface with the $\sqrt{3}\times\sqrt{3}$ periodic arrangement of the Si adatoms is still visible. A stable adsorption of the molecules on the surface is observed. When the same area is scanned repeatedly, no changes in the positions of the molecules occur. Sudden (dis)appearances of bright spots from one scanline to the following one as indicated by white circles in Figures 3A and C are only rarely observed. As they happen directly while the respective molecule is scanned, they are assigned to movements induced by an interaction with the STM tip.

In Figure 3B, a more detailed STM image of the IPr-NHO sample is shown. Such STM images of isolated molecules with atomic resolution on the surrounding substrate allow the determination of the adsorption site. The
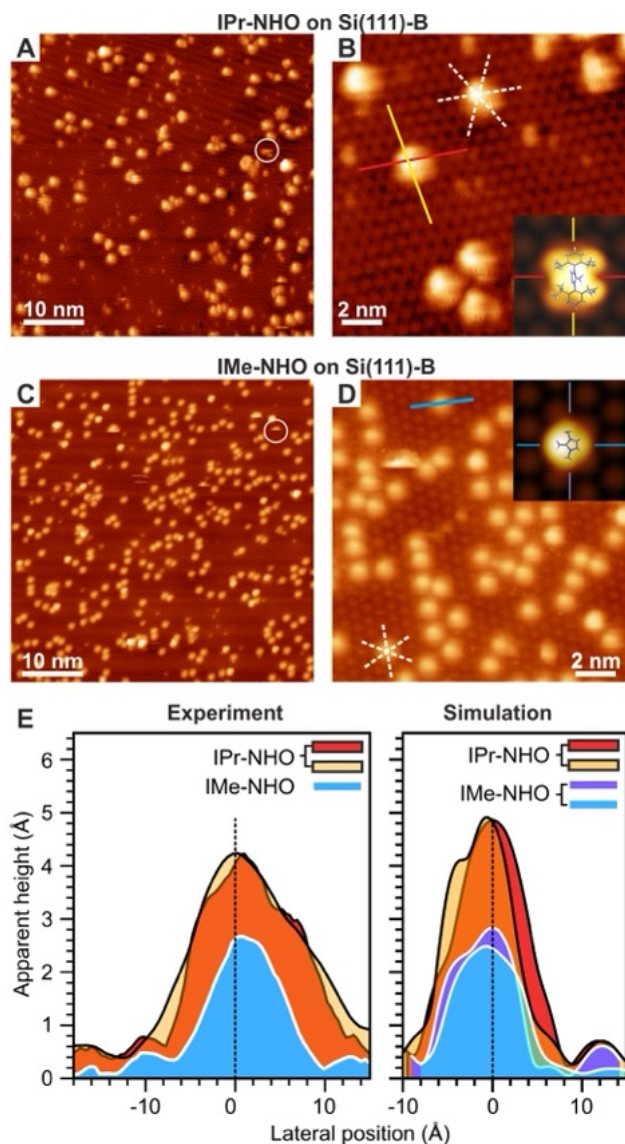
Figure 3. (A,B) STM results for a low coverage of IPr-NHO on Si(111)-B. (A) Overview STM image (sample voltage $V_T = -2.8$ V; tunneling current $I_T = 20$ pA) and (B) detailed STM image ($V_T = -2.8$ V; $I_T = 20$ pA). (C,D) STM results for a low coverage of IMe-NHO on Si(111)-B. (C) Overview STM image ($V_T = -2.5$ V; $I_T = 10$ pA) and (D) detailed STM image ($V_T = -2.0$ V; $I_T = 10$ pA). (E) Comparison between experimental and calculated height profiles extracted along the lines indicated in (B) and (D). For IMe-NHO, only one experimental profile is shown as the molecules appear round due to their free rotation.

positions of the Si adatom rows relevant for one IPr-NHO molecule are indicated by white dashed lines. The crossing point is located in the center of the molecule showing that the molecules indeed adsorb on top of the Si adatoms of the substrate as predicted by the theory results presented above. Figure 3D shows corresponding detailed STM data for the IMe-NHO sample. The insets in B and D show simulated STM images of the two molecules on Si(111)-B.

To investigate if the STM images are able to support DFT findings of different adsorption geometries (upright vs. flat lying) for IPr-NHO and IMe-NHO, height profiles are

extracted for both molecules. The results are shown in Figure 3E. For IPr-NHO, a height of 3.6 ± 0.5 Å above the adatoms is measured. This apparent height is compared with the simulated apparent height profile (taken along the lines indicated in the insets in Figure 3B,D) on the basis of the DFT geometry as shown on the right hand side in Figure 3E. The good agreement strongly points towards the theoretically found upright adsorption geometry. Also the smaller height of ~3 Å found for the corresponding NHC on the same substrate nicely agrees:[19] Due to the exocyclic CH_2 group, a smaller height is expected for NHCs as compared to NHOs.

On the other hand, the observed width of the IPr-NHO molecule of 13 Å (FWHM) is comparable with the geometric one (11.9 Å) and with that found for the corresponding (upright) NHC.[19] The slightly narrower profile in the simulation as compared to the experiment is assigned to rotational vibrations of the molecules coupled with vibrations of the N-substituents.

For IMe-NHO, an apparent height of 2.2 ± 0.3 Å is found, which is considerably lower than the value determined for IPr-NHO. For an equivalent upright adsorption geometry similar values would be expected for IMe-NHO and IPr-NHO, thus the lower value found here points towards a different geometry, in agreement with theory (Figure 2). Indeed, a comparison of the simulated height profiles for IPr-NHO and IMe-NHO gives very similar results (see Figure 3E, right hand side).

Our STM data can furthermore validate the above theoretical findings regarding the azimuthal rotation of the molecules. Regarding IMe-NHO, the round appearance of the STM image without any resolution of the inner structure of the molecule (see Figure 3D) can first of all be related to the free rotation of the molecules, which is too fast to be resolved in STM leading to the round shape. Second, as demonstrated by the dashed white lines drawn along the adatom row directions in Figure 3D, the center is again found on top of the adatoms. This directly shows that the STM appearance represents the time averaged image of the rotating molecules, as in the case of static molecules one would expect the center of the STM feature to be located to the side of an adatom. And third, the larger experimental width of IMe-NHO (~9 Å) in comparison to the simulated one (~7 Å) can also be related to this phenomenon (see Figure 3E). For IPr-NHO on the other hand, a more structured appearance is observed. In this case different orientations of molecules can also be distinguished in Figure 3B. These findings point towards a more static adsorption in agreement with the larger energy barrier for rotation found in the calculations (see Figure S2).

A key question to be answered is: are the adsorbed molecules better represented by the neutral olefinic or the zwitterionic ylide resonance structure? In the following we demonstrate that both upright and flat binding modes are best characterized by the ylide form. First, as reported in Figure 4, the C_{endo}–C_{exo} bond length of IMe-NHO increases upon adsorption (from 1.36 Å to 1.45 Å) and C_{exo} adopts a geometry consistent with sp^3-hybridization ($\angle Si$–C_{exo}–$C_{endo} = 104.2°$). Both of these changes are characteristic of a double-
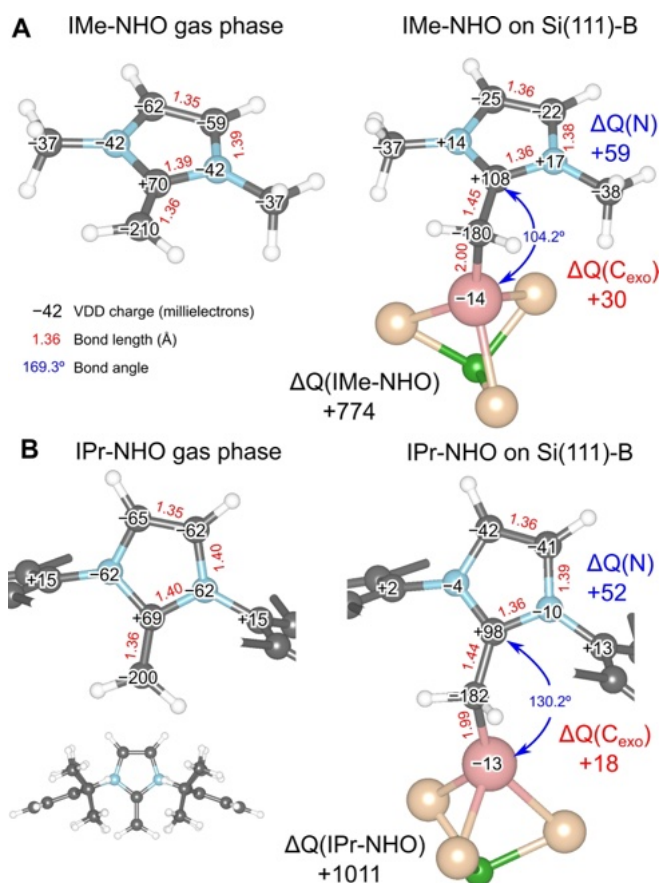
Figure 4. Voronoi deformation density (VDD) atomic charges and charge differences ΔQ (millielectrons), bond lengths (Å), and internal angles (degrees) for (A) IMe-NHO and (B) IPr-NHO, in gas phase and after adsorption on the Si(111)-B surface. The IPr-NHO side groups have been hidden for clarity (see inset).

to-single C–C bond transformation. Although the corresponding angle in IPr-NHO is larger (130.2°), this is imposed by the steric interaction of the large side groups with the silicon surface; the change in bond character is nonetheless reflected by the extension of C_{endo}–C_{exo} to 1.44 Å also in this case. Moreover, analysis of the atomic charges computed with the Voronoi deformation density (VDD)[67] approach (Figure 4 and Figure S5) indicates that the N atoms exhibit a relatively larger positive partial charge ΔQ after adsorption on the surface, which is consistent with the resonance structure of the ylide (Figure 1).

Second, analysis of the electron localization function (ELF) yields direct evidence of a double-to-single bond transformation. It has been reported that the ELF of C–C and C=C bonds have a very different spatial character: while the C–C bond has a round isosurface, the C=C bond is distinguished by a dumbbell shape with a larger extension perpendicular to the bond.[68,69] These characteristics are clearly observed for both C=C bonds present in the gas-phase IMe-NHO molecule (Figure 5A–C). On adsorption, while the backbone C=C bond remains, the C_{exo}–C_{endo} bond appears more localized and rounded, as befits the C–C
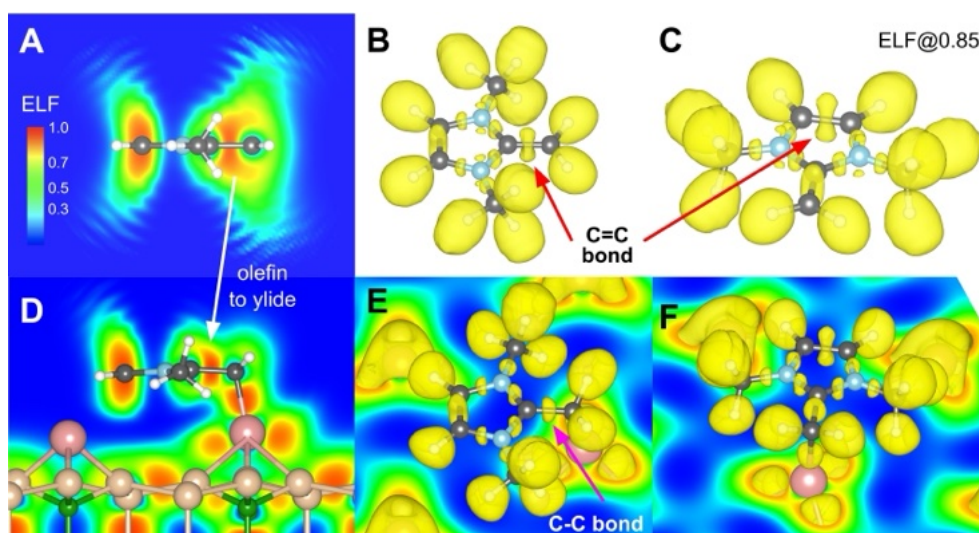
Figure 5. (A) Electron localization function (ELF) for gas phase IMe-NHO. The plane intersects the C_{exo} and C_{endo} atoms and lies perpendicular to the central ring. (B,C) Isosurfaces for ELF at 0.85, a value which corresponds to high electron density. (D–F) As (A–C) for IMe-NHO adsorbed on Si(111)-B. A horizontal plane intersecting the Si adatoms has been added for clarity in panels (E,F).

character. This is observed for both vertical and flat-on binding modes: see also Figure S3 for the IPr-NHO case.

At higher molecular coverages, monolayers of NHOs form on the surface. We start with the discussion of the STM results for IMe-NHO. Figure 6A shows an overview STM image of a silicon sample covered with a monolayer of IMe-NHO. The molecules appear with similar height indicating a homogeneous growth. This is in agreement with our DFT results showing that even for higher coverages the molecules still adopt the same flat-lying geometry as in the low coverage case (see Figure S4). The monolayer does not show a long range ordering, only occasionally small clusters with either hexagonal or rectangular arrangement are found as indicated in the more detailed STM image shown in Figure 6B. Here, different periodicities are observed: The regions marked green and blue correspond to hexagonally ordered patches with $2\sqrt{3} \times 2\sqrt{3}$ or 3×3 periodicity, respectively. The yellow boxes mark patches with a rectangular arrangement of the molecules leading to 3 different orientations due to the substrate symmetry. Here, a $3 \times 2\sqrt{3}$ periodicity is found. For each ordering, an example unit cell is indicated. Nevertheless, molecules with a closer distance corresponding to $\sqrt{3}$ are also observed, as indicated by the white boxes. Possible geometries and a comparison of simulated and experimental STM images for the ordered patches are shown in Figures S4 and S7.

To gain further insights into the properties of the IMe-NHO monolayer, X-ray photoelectron spectroscopy (XPS) measurements were additionally performed. The results for the C 1s and N 1s core levels are shown in Figure 6E, Figure S8, and Figure S9. The C 1s spectrum is relatively broad and consists of a double peak structure. According to the molecular structure, it is decomposed into four components, two with single intensity corresponding to C_{exo} and C_{endo} and two with double intensity corresponding to the C atoms in the methyl groups and the backbone. The resulting
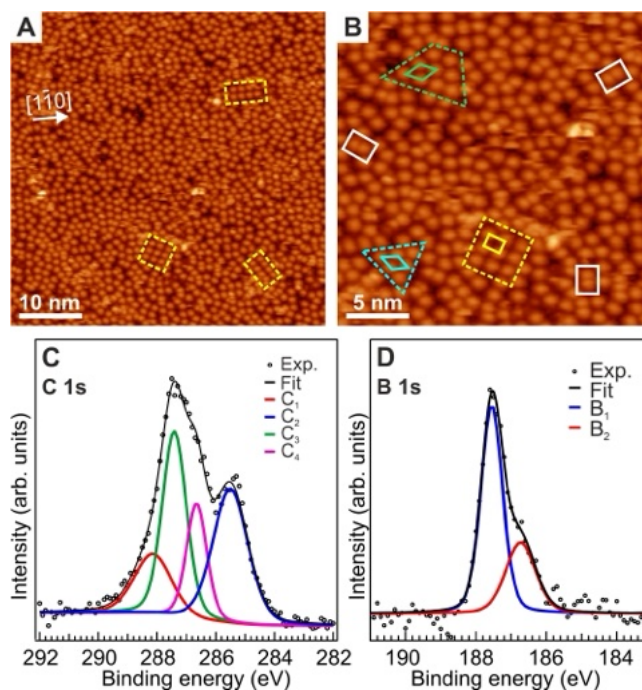
Figure 6. (A) Overview ($V_T = -2.0$ V; $I_T = 10$ pA) and (B) more detailed STM image ($V_T = -2.0$ V; $I_T = 10$ pA) of the IMe-NHO monolayer on Si(111)-B. In (B) small ordered patches with an ordered hexagonal $2\sqrt{3} \times 2\sqrt{3}$ or 3×3 or rectangular $3 \times 2\sqrt{3}$ arrangement are indicated together with the corresponding unit cells in green, blue, and yellow, respectively. The white boxes mark pairs of molecules with $\sqrt{3}$ distance. For the rectangular arrangement three orientations exist, as indicated in (A). (C,D) XPS results for (C) the C 1s core level and (D) the B 1s core level.

fit is shown as a black line in Figure 6C. The detailed assignment of the components and the exact core-level shifts (CLSs) are given in Figure S8. The spectrum differs consid-

erably from the one measured in Ref. [19] for upright IMe-NHCs again supporting the conclusion of a different adsorption geometry: the larger CLSs together with the additional component C_4 from C_{exo} lead to a considerably larger overall width of the spectrum being assigned to the larger molecule substrate interaction in the flat-lying geometry. The energetic position of the C_1 and C_4 components stemming from C_{endo} and C_{exo} thereby is in accordance with the ylidic character: The large negative (positive) charge at $C_{exo}(C_{endo})$ (see Figures 4 and S5) lead to a larger (weaker) screening of the nuclear coulomb potential and finally the observed lower (higher) binding energy. The N 1s spectrum in Figure S9 shows a single component at 402.1 eV binding energy.

From STM overview images like the one shown in Figure 6A, the experimental coverage of the IMe-NHO monolayer is determined. Hereon, we define the coverage as the percentage of molecules adsorbed per Si adatom, i.e. per $\sqrt{3} \times \sqrt{3}$ cell. From the STM data, a value of $31 \pm 5\%$ is determined. The B 1s core-level spectra offer a further possibility to determine the actual molecular coverage as demonstrated in our previous work on NHCs.[19] As shown in Figures 6D and S10, the B 1s core level consisting of only one component for the clean Si(111)-B surface splits into two chemically shifted ones for the NHO covered surface: One component B_1 again corresponding to B atoms underneath Si adatoms not binding to molecules and the other

component B_2 corresponding to those B atoms underneath Si adatoms binding to the molecules. The latter is shifted due to the interaction with the NHO molecules. From the intensity ratio between the two components, the coverage is determined revealing that $32 \pm 5\%$ of the adatoms are covered with molecules, in good agreement with the STM data.

It is interesting to note that higher coverages of 50% and even 75% are well energetically possible if one assumes local adsorption geometries like those shown in Figure S4. However, the calculated rotational barrier is very low, about 70 meV, as shown in Figure S2. Thus we expect large thermal fluctuations in the local orientations, which can influence (impede) the formation of larger or denser ordered domains.

Figure 7A shows an overview STM image of a silicon sample covered with a complete monolayer of IPr-NHO. Here, ordered domains are observed, in which the IPr-NHO molecules form a hexagonal arrangement. In Figure 7B, a more detailed image is shown. From the height profile taken along the blue line (see Figure 7C), a distance of 13.2 Å is determined, corresponding to twice the adatom distance. Thus, the IPr-NHO molecules arrange with a $2\sqrt{3} \times 2\sqrt{3}$ R30°-periodicity as shown in (D). DFT calculations at this coverage reveal that the IPr-NHO molecules again align with their wingtips lying between pairs of Si adatoms, allowing three equivalent alignments, in a geometry very
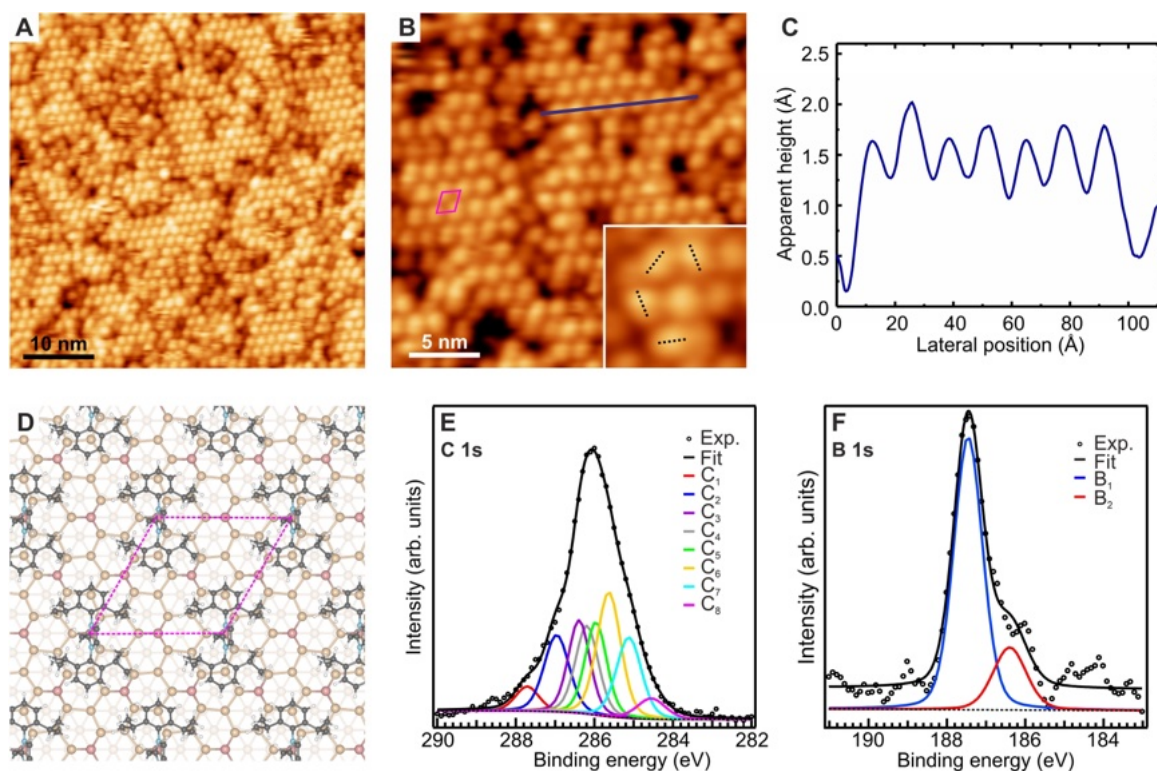
Figure 7. STM, DFT, and XPS results for the IPr-NHO monolayer. (A) Overview ($V_T = +3.0$ V; $I_T = 15$ pA) and (B) detailed STM images ($V_T = +3.0$ V; $I_T = 15$ pA) of the ordered IPr-NHO monolayer. In (B), a $2\sqrt{3} \times 2\sqrt{3}$ unit cell is indicated, the inset shows a small area in which the three possible orientations of the molecules are visible. (C) Height profile along the blue line in (B) showing the $2\sqrt{3}$-periodicity. (D) Geometry of the IPr-NHO monolayer as obtained from the DFT calculations. (E,F) XPS results for (E) the C 1s core level and (F) the B 1s core level.

similar to the isolated case. The presence of nearby molecules, however, makes hopping to an adjacent Si adatom site impossible, and further restricts rotation around the bond axis. As a result of the lower translational and rotational freedom, the STM images appear better resolved showing elongated spots. Due to the substrate symmetry, three orientations are observed, as indicated in the inset in Figure 7B.

To gain further insights into the properties of the IPr-NHO layer on Si(111)-B, XPS measurements were performed again. The results for the C $1s$ and N $1s$ core levels are shown in Figure 7E and Figure S9, respectively. In contrast to the results for IMe-NHO discussed above, the lineshape of the C $1s$ core-level spectrum in the IPr-NHO case is very similar to the one measured for the corresponding NHC.[19] This is particularly obvious when looking at the fit shown in Figure 7E, which is obtained using the same components as in Ref. [19] and an additional one for C_{exo}. The detailed assignment of the components and the exact values for the CLSs are given in Figure S12. This observation further supports the above conclusion of a similar upright adsorption geometry as for the corresponding NHC. A different geometry should lead to a different interaction with the surface and thus to different CLSs similar as observed for IMe-NHO. Only the obvious difference between the NHO and the NHC regarding the binding to the surface and the ylidic character is visible in the energetic positions of the C_1 component and the C_8 component assigned to C_{exo} and C_{endo}, respectively. Component C_8 (C_{exo}) is located on the low binding energy side, again assigned to the larger screening of the nuclear coulomb potential due to the negative charge, while the positive charge at C_{endo} leads to a larger binding energy (see also Figures 4 and S5). The N $1s$ core-level (Figure S9) again shows a single component at 402.7 eV binding energy.

The observed $2\sqrt{3} \times 2\sqrt{3}$-periodicity means that one IPr-NHO molecule binds per four substrate Si adatoms. However, on the real surface also domain boundaries and other defects are present where the local density of molecules is lower as compared to the 25 % for the ideal $2\sqrt{3} \times 2\sqrt{3}$ monolayer. This leads to a slightly lower overall coverage. When analyzing STM images of the monolayer like the one shown in Figure 7A, a coverage of 22 ± 5 % is obtained. As done before for IMe-NHO, the experimental coverage of the IMe-NHO monolayer is additionally determined on the basis of B $1s$ spectra shown in Figures 7F and S10 giving a coverage of 21 ± 5 % in good agreement with the STM results.

The Si $2p$ core-level was also measured. Spectra for the IMe-NHO and IPr-NHO monolayers are shown in Figure S11 revealing changes in band banding upon molecule adsorption.

It should be noted that our measurements strongly suggest that the stable NHO coverage saturates at full monolayers and no NHO multilayer growth occurs: first, in STM we observe a very homogeneous height distribution for the monolayers without any additional NHO islands on top. All steps show heights corresponding to multitudes of single Si(111) step heights. And second, the intensity in the C $1s$

spectra measured for a series of NHO coverages shows a clear saturation behavior (Figure S13).

NHC monolayers on silicon are characterized by a high thermal stability and large work function reductions both being important prerequisites for a successful application e.g. in (opto)electronic devices.[19,20] To investigate if NHO films on Si(111)-B exhibit similar or even superior properties, corresponding measurements and calculations were performed.

The work function change is determined experimentally by measuring the secondary electron onsets for the clean Si(111)-B surface, for the IPr-NHO monolayer, and for the IMe-NHO monolayer on Si(111)-B using XPS (see Figure S14). For the IPr-NHO monolayer, a reduction of 1.61 ± 0.19 eV with respect to clean Si(111)-B is found; a slightly higher value of 1.71 ± 0.19 eV is found for the IMe-NHO monolayer. To understand how these values depend on the different molecular coverages and adsorption geometries, we compare them in Figure 8A with calculated work function changes across a range of coverages (see Figure S4 for the corresponding geometries). The computed results
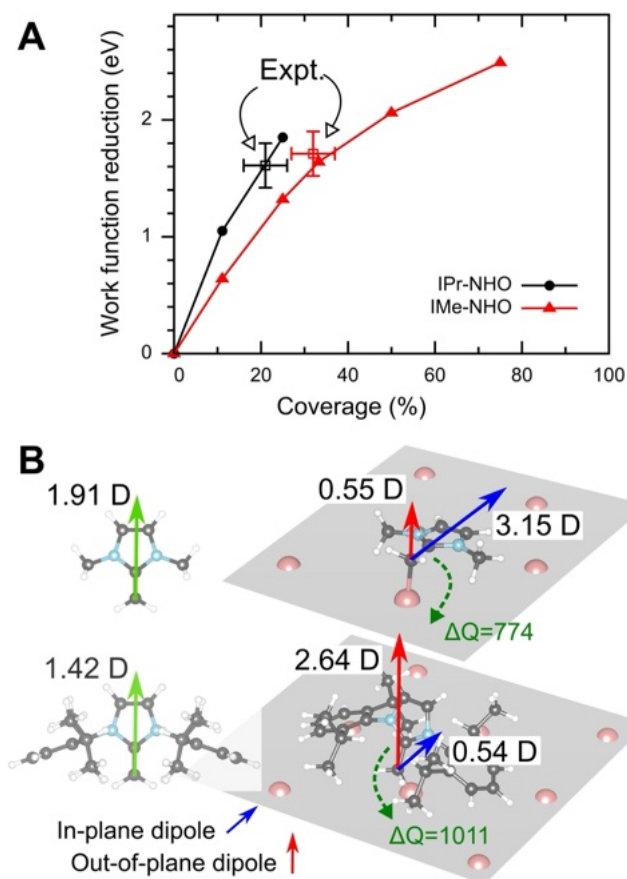
Figure 8. (A) Calculated work function reduction for NHO layers on Si(111)-B as a function of molecular coverage per Si adatom, along with experimental data. (B) Dipole moments of (left) gas-phase NHOs and (right) adsorbed NHO fragments (i.e., molecules in the adsorbed geometry, without substrate). In-plane (blue) and out-of-plane (red) components are reported in debye. The total charge transfer ΔQ to the surface (in millielectrons) is indicated.

are found to be in good agreement with the measured data at the corresponding coverages, indicating that the higher measured work function reduction for the IMe-NHO monolayer is simply due to its higher surface density. Instead, for an equivalent coverage, the reduction is 40–60 % larger for IPr-NHO.

The different work function reductions can be explained by considering the nature of the charge transfer and the dipole formation at the NHO/silicon interface, as summarized in Figure 8B. Firstly, adsorption of IPr-NHO leads to a larger overall transfer of electrons to the surface (1.01 compared with 0.77 for IMe-NHO). As shown in Figure S6, this induces a strong dipole centred at the Si–C_{exo} bond, causing a potential drop. Secondly, the upright and flat-lying binding geometries introduce different intrinsic dipoles at the surface. While IPr-NHO has a smaller dipole moment (1.42 D) than IMe-NHO in the gas phase, when adsorbed it introduces a much larger dipole moment of 2.64 D along the surface normal, with only a small lateral component induced by the moderate tilt angle. In contrast, the IMe-NHO dipole lies almost completely parallel to the surface plane so that the out-of-plane dipole component is strongly reduced. As a result, the impact on the surface work function is lower for the smaller NHO. This behaviour is in stark contrast to the corresponding NHCs, where a similar trend in the work function reduction was found for both IMe and IPr.[19] Indeed, both NHCs adsorb on Si(111)-B with similar upright geometries.

Incidentally, the large in-plane dipole associated with the adsorbed IMe-NHO geometry may help explain why formation of large and dense ordered domains is not observed. As shown in Figure S4, 33 % corresponds to the highest possible coverage for which the molecular dipoles can align in a head-to-tail geometry. Instead, coverages of 50 % or 75 % necessarily feature head-to-head or side-on alignments. Such dipole-dipole interactions are less favoured, as suggested by the drop in average adsorption energy (reported in Figure S4), and may further impact the kinetic processes required for the formation of such dense, ordered domains.

The high thermal stability of NHCs on metals[24,26,28,41] and semiconductors[19] is another important property, also in regard to possible applications of the films. Like in our previous work on NHCs, we measured the thermal stability of the IPr-NHO and IMe-NHO monolayers using the C 1s core-level for several annealing steps between 100 °C and 250 °C (see Figure S15).

The IMe-NHO monolayer remains stable on the surface up to temperatures of at least 150 °C, while only a slight decrease in intensity assigned to desorption of some molecules is observed. At higher temperatures, the spectral shape changes considerably indicating a decomposition of the molecules. For IPr-NHO, a similar behavior is observed with the intensity staying almost constant and without distinct changes in the spectral shape occurring up to 150 °C. These observations are consistent with the computed (average) adsorption energies at the monolayer coverages: −1.68 eV for IMe-NHO at 33 % and −1.90 eV for IPr-NHO at 25 % coverage per adatom. The thermal stabilities found

here are comparable to the values reported for NHCs on metals and semiconductors, for which similar onsets of the desorption in the range from 190–230 °C were reported.[19,26,28]

These results demonstrate that the adsorption geometry has a strong influence on the properties of the NHO monolayers with upright molecules leading to larger changes in the work function.

Conclusion

The adsorption behavior of two model N-heterocyclic olefins on Si(111)-B was investigated in detail using STM, XPS, and DFT. Both NHOs adsorb through an ylide binding mode and form covalent bonds with substrate Si adatoms. The adsorption geometries differ, however, depending on the steric encumbrance of the N-substituents. The larger IPr-NHO adsorbs in a vertical geometry leading to the formation of ordered monolayers with $2\sqrt{3} \times 2\sqrt{3}$ periodicity. Instead, IMe-NHO binds in a flat-lying geometry and forms a slightly more tightly packed, but disordered, monolayer. Both monolayers are characterized by large workfunction reductions and good thermal stabilities, comparable to those of NHCs on surfaces. Our demonstration of the first reported adsorption geometry of different NHOs on a surface, together with the preferable interaction through the ylide form to Si, will be of great prospect in designing tailor-made ligand structures for future applications in organic electronics and optoelectronics, catalysis, and material science.

Conflict of Interest

The authors declare no conflict of interest.

Data Availability Statement

The data that support the findings of this study are available from the corresponding authors upon reasonable request.

[1] S. F. Bent, *J. Phys. Chem. B* **2002**, *106*, 2830.

[2] A. Vilan, O. Yaffe, A. Biller, A. Salomon, A. Kahn, D. Cahen, *Adv. Mater.* **2010**, *22*, 140.

[3] M. M. D. Roy, E. Rivard, *Acc. Chem. Res.* **2017**, *50*, 2017.

[4] A. Doddi, M. Peters, M. Tamm, *Chem. Rev.* **2019**, *119*, 6994.

[5] N. Kuhn, H. Bohnen, J. Kreutzberg, D. Bläser, R. Boese, *J. Chem. Soc. Chem. Commun.* **1993**, *1993*, 1136.

[6] N. Kuhn, M. Steimann, G. Weyers, *Z. Naturforsch. B* **1999**, *54*, 427.

[7] A. Dumrath, X.-F. Wu, H. Neumann, A. Spannenberg, R. Jackstell, M. Beller, *Angew. Chem. Int. Ed.* **2010**, *49*, 8988.

[8] S. Naumann, *Chem. Commun.* **2019**, *55*, 11658.

[9] Y.-B. Wang, D.-S. Sun, H. Zhou, W.-Z. Zhang, X.-B. Lu, *Green Chem.* **2015**, *17*, 4009.

[10] I. C. Watson, A. Schumann, H. Yu, E. C. Davy, R. Mc-Donald, M. J. Ferguson, C. Hering-Junghans, E. Rivard, *Chem. Eur. J.* **2019**, *25*, 9678.

[11] M. Schedler, N. E. Wurz, C. G. Daniliuc, F. Glorius, *Org. Lett.* **2014**, *16*, 3134.

[12] B. Maji, H. Mayr, *Angew. Chem. Int. Ed.* **2012**, *51*, 10408.

[13] B. Maji, M. Horn, H. Mayr, *Angew. Chem. Int. Ed.* **2012**, *51*, 6231.

[14] A. T. Biju, M. Padmanaban, N. E. Wurz, F. Glorius, *Angew. Chem. Int. Ed.* **2011**, *50*, 8412.

[15] C. E. I. Knappke, J. M. Neudörfl, A. J. von Wangelin, *Org. Biomol. Chem.* **2010**, *8*, 1695.

[16] A. Fürstner, M. Alcarazo, R. Goddard, C. W. Lehmann, *Angew. Chem. Int. Ed.* **2008**, *47*, 3210.

[17] K. Powers, C. Hering-Junghans, R. McDonald, M. J. Ferguson, E. Rivard, *Polyhedron* **2016**, *108*, 8.

[18] R. Dorta, E. D. Stevens, N. M. Scott, C. Costabile, L. Cavallo, C. D. Hoff, S. P. Nolan, *J. Am. Chem. Soc.* **2005**, *127*, 2485.

[19] M. Franz, S. Chandola, M. Koy, R. Zielinski, H. Aldahhak, M. Das, M. Freitag, U. Gerstmann, D. Liebig, A. K. Hoffmann, M. Rosin, W. G. Schmidt, C. Hogan, F. Glorius, N. Esser, M. Dähne, *Nat. Chem.* **2021**, *13*, 828–835.

[20] R. Zielinski, M. Das, C. Kosbab, M. T. Nehring, M. Dähne, N. Esser, M. Franz, F. Glorius, *J. Mater. Chem. C* **2023**, *11*, 7377.

[21] K. V. S. Ranganath, J. Kloesges, A. H. Schäfer, F. Glorius, *Angew. Chem. Int. Ed.* **2010**, *49*, 7786.

[22] A. V. Zhukhovitskiy, M. G. Mavros, T. Van Voorhis, J. A. Johnson, *J. Am. Chem. Soc.* **2013**, *135*, 7418.

[23] M. N. Hopkinson, C. Richter, M. Schedler, F. Glorius, *Nature* **2014**, *510*, 485.

[24] C. M. Crudden, J. H. Horton, I. I. Ebralidze, O. V. Zenkina, A. B. McLean, B. Drevniok, Z. She, H.-B. Kraatz, N. J. Mosey, T. Seki, E. C. Keske, J. D. Leake, A. Rousina-Webb, G. Wu, *Nat. Chem.* **2014**, *6*, 409.

[25] A. V. Zhukhovitskiy, M. J. MacLeod, J. A. Johnson, *Chem. Rev.* **2015**, *115*, 11503.

[26] C. M. Crudden, J. H. Horton, M. R. Narouz, Z. Li, C. A. Smith, K. Munro, C. J. Baddeley, C. R. Larrea, B. Drevniok, B. Thanabalasingam, A. B. McLean, O. V. Zenkina, I. I. Ebralidze, Z. She, H.-B. Kraatz, N. J. Mosey, L. N. Saunders, A. Yagi, *Nat. Commun.* **2016**, *7*, 12654.

[27] G. Wang, A. Rühling, S. Amirjalayer, M. Knor, J. B. Ernst, C. Richter, H.-J. Gao, A. Timmer, H.-Y. Gao, N. L. Doltsinis, F. Glorius, H. Fuchs, *Nat. Chem.* **2017**, *9*, 152.

[28] C. R. Larrea, C. J. Baddeley, M. R. Narouz, N. J. Mosey, J. H. Horton, C. M. Crudden, *ChemPhysChem* **2017**, *18*, 3536.

[29] L. Jiang, B. Zhang, G. Medard, A. P. Seitsonen, F. Haag, F. Allegretti, J. Reichert, B. Kuster, J. V. Barth, A. C. Papageorgiou, *Chem. Sci.* **2017**, *8*, 8301.

[30] Z. Li, K. Munro, I. I. Ebralize, M. R. Narouz, J. D. Padmos, H. Hao, C. M. Crudden, J. H. Horton, *Langmuir* **2017**, *33*, 13936.

[31] J. B. Ernst, C. Schwermann, G.-i. Yokota, M. Tada, S. Muratsugu, N. L. Doltsinis, F. Glorius, *J. Am. Chem. Soc.* **2017**, *139*, 9144.

[32] C.-Y. Wu, W. J. Wolf, Y. Levartovsky, H. A. Bechtel, M. C. Martin, F. D. Toste, E. Gross, *Nature* **2017**, *541*, 511.

[33] E. A. Doud, M. S. Inkpen, G. Lovat, E. Montes, D. W. Paley, M. L. Steigerwald, H. Vázquez, L. Venkataraman, X. Roy, *J. Am. Chem. Soc.* **2018**, *140*, 8944.

[34] M. Trujillo, S. L. Strausser, J. C. Becca, J. F. DeJesus, L. Jensen, D. M. Jenkins, J. P. Camden, *J. Phys. Chem. Lett.* **2018**, *9*, 6779.

[35] D. T. Nguyen, M. Freitag, M. Körsgen, S. Lamping, A. Rühling, A. H. Schäfer, M. H. Siekman, H. F. Arlinghaus, W. G. van der Wiel, F. Glorius, B. J. Ravoo, *Angew. Chem. Int. Ed.* **2018**, *57*, 11465.

[36] G. Lovat, E. A. Doud, D. Lu, G. Kladnik, M. S. Inkpen, M. L. Steigerwald, D. Cvetko, M. S. Hybertsen, A. Morgante, X. Roy, L. Venkataraman, *Chem. Sci.* **2019**, *10*, 930.

[37] C. A. Smith, M. R. Narouz, P. A. Lummis, I. Singh, A. Nazemi, C.-H. Li, C. M. Crudden, *Chem. Rev.* **2019**, *119*, 4986.

[38] M. R. Narouz, K. M. Osten, P. J. Unsworth, R. W. Y. Man, K. Salorinne, S. Takano, R. Tomihara, S. Kaappa, S. Malola, C.-T. Dinh, J. D. Padmos, K. Ayoo, P. J. Garrett, M. Nambo, J. H. Horton, E. H. Sargent, H. Häkkinen, T. Tsukuda, C. M. Crudden, *Nat. Chem.* **2019**, *11*, 419.

[39] E. A. Doud, R. L. Starr, G. Kladnik, A. Voevodin, E. Montes, N. P. Arasu, Y. Zang, P. Zahl, A. Morgante, L. Venkataraman, H. Vázquez, D. Cvetko, X. Roy, *J. Am. Chem. Soc.* **2020**, *142*, 19902.

[40] E. Amit, L. Dery, S. Dery, S. Kim, A. Roy, Q. Hu, V. Gutkin, H. Eisenberg, T. Stein, D. Mandler, F. Dean Toste, E. Gross, *Nat. Commun.* **2020**, *11*, 5714.

[41] A. Krzykawska, M. Wróbel, K. Kozieł, P. Cyganik, *ACS Nano* **2020**, *14*, 6043.

[42] P. Bellotti, M. Koy, M. N. Hopkinson, F. Glorius, *Nat. Chem. Rev.* **2021**, *5*, 711.

[43] M. Koy, P. Bellotti, M. Das, F. Glorius, *Nat. Catal.* **2021**, *4*, 352.

[44] A. Inayeh, R. R. K. Groome, I. Singh, A. J. Veinot, F. C. de Lima, R. H. Miwa, C. M. Crudden, A. B. McLean, *Nat. Commun.* **2021**, *12*, 4034.

[45] P. Knecht, B. Zhang, J. Reichert, D. A. Duncan, M. Schwarz, F. Haag, P. T. P. Ryan, T.-L. Lee, P. S. Deimel, P. Feulner, F. Allegretti, W. Auwärter, G. Médard, A. P. Seitsonen, J. V. Barth, A. C. Papageorgiou, *J. Am. Chem. Soc.* **2021**, *143*, 4433.

[46] I. Berg, L. Hale, M. Carmiel-Kostan, F. D. Toste, E. Gross, *Chem. Commun.* **2021**, *57*, 5342.

[47] I. Berg, E. Amit, L. Hale, F. D. Toste, E. Gross, *Angew. Chem. Int. Ed.* **2022**, *61*, e202201093.

[48] P. Knecht, D. Meier, J. Reichert, D. A. Duncan, M. Schwarz, J. T. Küchle, T.-L. Lee, P. S. Deimel, P. Feulner, F. Allegretti, W. Auwärter, G. Médard, A. P. Seitsonen, J. V. Barth, A. C. Papageorgiou, *Angew. Chem. Int. Ed.* **2022**, *61*, e202211877.

[49] Y. Choi, C. S. Park, H.-V. Tran, C.-H. Li, C. M. Crudden, T. R. Lee, *ACS Appl. Mater. Interfaces* **2022**, *14*, 44969.

[50] E. Angove, F. Grillo, H. A. Früchtl, A. J. Veinot, I. Singh, J. H. Horton, C. M. Crudden, C. J. Baddeley, *J. Phys. Chem. Lett.* **2022**, *13*, 2051.

[51] G. Kaur, R. L. Thimes, J. P. Camden, D. M. Jenkins, *Chem. Commun.* **2022**, *58*, 13188.

[52] R. J. Lewis, M. Koy, M. Macino, M. Das, J. H. Carter, D. J. Morgan, T. E. Davies, J. B. Ernst, S. J. Freakley, F. Glorius, G. J. Hutchings, *J. Am. Chem. Soc.* **2022**, *144*, 15431.

[53] A. V. Zhukhovitskiy, M. G. Mavros, K. T. Queeney, T. Wu, T. V. Voorhis, J. A. Johnson, *J. Am. Chem. Soc.* **2016**, *138*, 8639.

[54] B. Baris, V. Luzet, E. Duverger, P. Sonnet, F. Palmino, F. Cherioux, *Angew. Chem. Int. Ed.* **2011**, *50*, 4094.

[55] S. R. Wagner, R. R. Lunt, P. Zhang, *Phys. Rev. Lett.* **2013**, *110*, 086107.

[56] O. Guillermet, A. Mahmood, J. Yang, J. Echeverria, J. Jeannoutot, S. Gauthier, C. Joachim, F. Chérioux, F. Palmino, *ChemPhysChem* **2014**, *15*, 271.

[57] Y. Makoudi, J. Jeannoutot, F. Palmino, F. Cherioux, G. Copie, C. Krzeminski, F. Cleri, B. Grandidier, *Surf. Sci. Rep.* **2017**, *72*, 316.

[58] S. Lindner, M. Franz, M. Kubicki, S. Appelfeller, M. Dähne, H. Eisele, *Phys. Rev. B* **2019**, *100*, 245301.

[59] H. Aldahhak, C. Hogan, S. Lindner, S. Appelfeller, H. Eisele, W. G. Schmidt, M. Dähne, U. Gerstmann, M. Franz, *Phys. Rev. B* **2021**, *103*, 035303.

[60] M. Franz, *Inorg. Chim. Acta* **2024**, *559*, 121771.

[61] R. L. Headrick, I. K. Robinson, E. Vlieg, L. C. Feldman, *Phys. Rev. Lett.* **1989**, *63*, 1253.

[62] P. Bedrossian, R. D. Meade, K. Mortensen, D. M. Chen, J. A. Golovchenko, D. Vanderbilt, *Phys. Rev. Lett.* **1989**, *63*, 1257.

[63] M. Mas-Torrent, C. Rovira, *Chem. Rev.* **2011**, *111*, 4833.

[64] R. H. Friend, R. W. Gymer, A. B. Holmes, J. H. Burroughes, R. N. Marks, C. Taliani, D. D. C. Bradley, D. A. D. Santos, J. L. Brédas, M. Lögdlund, W. R. Salaneck, *Nature* **1999**, *397*, 121.

[65] W. Cao, J. Xue, *Energy Environ. Sci.* **2014**, *7*, 2123.

[66] H. K. Kim, A. S. Hyla, P. Winget, H. Li, C. M. Wyss, A. J. Jordan, F. A. Larrain, J. P. Sadighi, C. Fuentes-Hernandez, B. Kippelen, J.-L. Bredas, S. Barlow, S. R. Marder, *Chem. Mater.* **2017**, *29*, 3403.

[67] C. Fonseca Guerra, J.-W. Handgraaf, E. J. Baerends, F. M. Bickelhaupt, *J. Comput. Chem.* **2004**, *25*, 189.

[68] A. Savin, R. Nesper, S. Wengert, T. F. Fässler, *Angew. Chem. Int. Ed.* **1997**, *36*, 1808.

[69] K. Koumpouras, J. A. Larsson, *J. Phys. Condens. Matter* **2020**, *32*, 315502.